

RESEARCH PAPER

The role and mechanisms of zinc oxide nanoparticles in the improvement of the radiosensitivity of lung cancer cells in clinically relevant megavoltage radiation energies in-vitro

Masoumeh Zangeneh¹, Hassan Ali Nedaei^{1, 2*}, Hossein Mozdarani³, Aziz Mahmoudzadeh⁴, Sharmin Kharrazi⁵, Mahdieh Salimi⁶

¹Department of Medical Physics and Biomedical Engineering, School of Medicine, Tehran University of Medical Sciences, Tehran, Iran

²Department of Radiotherapy Oncology, Cancer Research Center, Cancer Institute, Tehran University of Medical Sciences, Tehran, Iran

³Department of Medical Genetics, Faculty of Medical Sciences, Tarbiat Modares University, Tehran, Iran

⁴Department of Biosciences and Biotechnology, Malek-Ashtar University of Technology, Tehran, Iran

⁵Department of Medical Nanotechnology, School of Advanced Technologies in Medicine, Tehran University of Medical Sciences, Tehran, Iran

⁶Institute of Medical Biotechnology, National Institute of Genetic Engineering and Biotechnology (NIGEB), Tehran, Iran

ABSTRACT

Objective(s): Semiconductor zinc oxide nanoparticles (ZnO NPs) have unique properties, such as inherent selectivity and photosensitization effects under ultraviolet (UV) radiation. ZnO NPs serve as promising anticancer agents. However, UV radiation limits their penetration into the body. In most clinical settings, it is essential to use high-energy photons in the treatment of deep-seated tumors. The present study aimed to evaluate the radiosensitization effects of ZnO NPs on human lung cancer cells under megavoltage (MV) X-ray irradiation.

Materials and Methods: ZnO NPs with the mean diameter of seven nanometers were synthesized and characterized. The cytotoxicity and cellular uptake of ZnO NPs were evaluated in SKLC-6 lung cancer and MRC-5 normal lung cells using the 3-(4,5-dimethylthiazol-yl)-5(3-carboxymethoxyphenyl)-2H-tetrazolium (MTT) and inductively coupled plasma-mass spectrometry assays, respectively. In addition, the radiosensitization effects of ZnO NPs were investigated under MV irradiation using a clonogenic survival assay. Apoptosis induction and DNA damage were also evaluated using flow cytometry and cytokinesis-block micronucleus assay, respectively.

Results: ZnO NPs were taken up and reduced the viability of the cancer cells at a higher rate compared to the normal cells. Moreover, ZnO NPs significantly enhanced the radiosensitivity of the cancer cells with the sensitizer enhancement ratios of 1.23 and 1.31 at the concentrations of 10 and 20 µg/ml, respectively. However, they had no significant effect on the radiosensitivity of the normal cells. Apoptosis induction and DNA damage also improved at a higher rate in the cancer cells compared to the normal cells with the combination of ZnO NPs with MV radiation.

Conclusion: According to the results, ZnO NPs had the potential to be a selective radiosensitizer for lung cancer radiotherapy under MV X-ray irradiation. Some of the cytotoxic and genotoxic mechanisms in radiosensitization by ZnO NPs were elevated apoptosis induction and DNA damage levels.

Keywords: Lung Cancer, Megavoltage Energy, Radiosensitization, Radiotherapy, ZnO Nanoparticles

How to cite this article

Zangeneh M, Nedaei H A, Mozdarani H, Mahmoudzadeh A, Kharrazi Sh, Salimi M. The role and mechanisms of zinc oxide nanoparticles in the improvement of the radiosensitivity of lung cancer cells in clinically relevant megavoltage radiation energies in-vitro. *Nanomed J.* 2019; 6(4): 276-290. DOI: 10.22038/nmj.2019.06.000006

* Corresponding Author Email: nedaieha@sina.tums.ac.ir

Note. This manuscript was submitted on May 14, 2019; approved on August 9, 2019

INTRODUCTION

Lung cancer is the most commonly diagnosed cancer, accounting for 11.6% of new cancer cases, and the leading cause of cancer mortality, constituting 18.4% of the total cancer deaths [1]. Radiotherapy has become a major approach to lung cancer treatment; however, the non-selective nature of ionizing radiations leads to inevitable damage to the surrounding healthy tissues, thereby causing severe complications, such as pneumonitis, pulmonary fibrosis, and cardiac toxicity [2, 3].

Several technological advances have aimed to deliver the maximum dose to tumor tissues while minimizing the dose of normal tissues, including three-dimensional conformal radiotherapy, intensity-modulated radiotherapy, image-guided radiotherapy, and stereotactic body radiation therapy [4].

Furthermore, radiosensitizer agents have been widely used to increase the effectiveness of radiotherapy through enhancing the radiosensitivity of tumor cells [5].

Recently, nanotechnology has introduced a wide variety of nanosystems, broadening the horizon for the development of efficient radiosensitizers. High atomic number (Z) nanoparticles (NPs), such as gold and gadolinium, have been most investigated to increase localized energy absorption and enhance the radiation dose in cancer cells [6]. Moreover, some low Z NPs have been reported to be effective radiosensitizers. Easy synthesis, cost-effectiveness, availability, and favorable biological properties are among the major advantages of low Z NPs as radiosensitizers. Some low Z NPs with efficient radiosensitization effects include iron oxide NPs [7], titanium oxide (TiO₂) NPs [8], carbon nanodots [9], and zinc oxide (ZnO) NPs [10, 11].

ZnO NPs are semiconductor materials with wide biomedical applications, including bio-imaging, bio-sensing, drug delivery, and cancer treatment [12]. ZnO NPs exhibit inherent selective toxicity toward cancer cells mainly through the regeneration of reactive oxygen species (ROS) [13]. This behavior is associated with the semiconductor properties of ZnO NPs. ZnO is a wide-bandgap semiconductor, which could reinforce photo-oxidation properties in combination with ultraviolet (UV) photons [14, 15]. The absorption of UV photons leads to the excitation of electrons (e⁻) in the valence band, promoting them to the conduction band that leaves the holes (h⁺) in the valence band. The electrons and holes that

are highly reactive could be transferred to the NP surface and react to the adsorbed oxygen or water molecules so as to produce superoxide (O₂⁻) and hydroxyl (OH[•]) radicals. Such generated ROSs are considered to be potent sensitizers for the photodestruction of cancer cells [13]. However, UV photons have an extremely shallow penetration depth in the body due to their low energy and are not used in the treatment of deep-seated tumors.

Some studies have indicated that ZnO NPs respond to X-ray photons at kilovoltage (kV) energy ranges to exert radiosensitization effects [10, 16]. Despite the significant radiosensitization, these studies have mostly been conducted under low-energy X-ray photons by applying low-energy X-rays sources, such as brachytherapy, intraoperative radiotherapy, and unsealed radioisotopes, which are mainly effective in the treatment of superficial tumors or the tumors that are close to the accessible cavities of the body [17].

In many clinical settings, it is essential to use high-energy or megavoltage (MV) photons to reach and treat the tumors that are located in the depths of the body and avoid skin damage.

In the present study, we demonstrated the potential of ZnO NPs for the radiosensitization of lung cancer cells using clinically relevant MV radiation beams, aiming to explore some of the cytotoxic and genotoxic mechanisms involved in ZnO NP radiosensitization. ZnO NPs with the mean diameter of seven nanometers were synthesized and characterized using several techniques. After determining cytotoxicity and cellular uptake, the possible radiosensitization (dose enhancement) of ZnO NPs was assessed using a clonogenic survival assay. In addition, the induction of apoptosis and DNA damage (in the micronuclei form) was investigated. In order to determine the possible selective radiosensitization of ZnO NPs, SKLC-6 lung carcinoma cells and MRC-5 normal lung fibroblast cells were selected as the target models, and the experiments were performed using cell culture *in-vitro*.

To the best of our knowledge, there have been limited studies on the radiosensitization effects of ZnO NPs under MV irradiation.

The results of the present study could contribute to the elucidation of ZnO NP radiosensitization effects and the relevant mechanisms for further translation into the clinical radiotherapy of lung cancer.

MATERIALS AND METHODS

NP preparation

In this study, ZnO NPs were prepared via the chemical precipitation route using zinc acetate dihydrate (Zn [CH₃CO₂]₂.2H₂O; Merck Chemicals, Germany) as the precursor, sodium hydroxide (NaOH; Merck Chemicals, Germany) as the reducing material, and methanol (Dr. Mojallali Chemical Complex Co., Iran) as the solvent.

Zinc acetate and sodium hydroxide were dissolved separately in methanol in order to obtain an aqueous solution at the concentrations of 0.2 M and 1.2 M, respectively and stirred using a magnetic stirrer at room temperature for one hour. Afterwards, the zinc acetate dihydrate solution was added drop-wise (rate: 5 ml/min) to the NaOH solution under continuous stirring, and the final mixture was vigorously stirred for an additional three hours at room temperature. The prepared solution containing ZnO NPs was centrifuged and washed five times in order to remove the unreacted precursors and dried at room temperature. Finally, the prepared ZnO NPs were ground using a mortar to form a powder.

NP characterization

The X-ray diffraction (XRD) patterns and crystalline phases of the prepared ZnO NPs were determined using an XRD diffractometer (model: EQuniox 3000, INEL, France). The general morphology and actual visual size of the synthesized ZnO NPs were examined via transmission electron microscopy (TEM; LEO, Zeiss, Germany). The ultraviolet-visible (UV-Vis) absorption spectrum of the ZnO NPs was recorded using a spectrophotometer (BioAquarius CE 7450, Cecil Instruments, UK).

The energy-dispersive X-ray analysis (EDAX) technique was used to determine the elemental purity of the prepared ZnO NPs using field-scanning electron microscopy (JSM-6500F, JEOL Inc. Japan), equipped with an energy dispersive spectrometer. To determine the colloidal stability of the ZnO NPs, hydrodynamic size and the surface charge (zeta potential) of the dispersed ZnO NPs were determined in some aqueous media, including deionized water, phosphate buffered saline (PBS; Gibco, Invitrogen, UK), and Dulbecco's modified eagle medium (DMEM; Gibco, Invitrogen, UK) supplemented with 5% and 10% fetal bovine serum (FBS; Gibco, Invitrogen, UK) at the concentration of 20 µg/ml. The media

were characterized by dynamic light scattering (DLS; Zetasizer Nano ZS90, Malvern Instrument, Worcestershire, United Kingdom).

Human cell Lines and cell culture conditions

SKLC-6 human lung carcinoma and MRC-5 human normal lung fibroblast cell lines were obtained from the National Cell Bank of the Pasteur Institute (Tehran, Iran) and cultured on DMEM supplemented with 10% FBS and 1% penicillin-streptomycin solution (Gibco, Invitrogen, UK). The cultures were preserved in a humidified incubator at the temperature of 37°C with 5% CO₂.

NP cytotoxicity evaluation using the MTT assay

The cytotoxicity of various concentrations of ZnO NPs was assessed in the cancer and normal cell lines using the 3-(4, 5-dimethylthiazol-2-yl)-2,5-diphenyltetrazolium bromide (MTT) assay. SKLC-6 and MRC-5 cells (density: 1/5×10⁴ cells/well) were seeded into 96-well plates in 100 microliters of the complete medium and incubated at the temperature of 37°C for 24 hours. Following that, ZnO NP concentrations of 0-100 µg/ml were added to each well. The control group received no NP treatment.

After 24 hours of incubation, the cells were washed twice using PBS. Afterwards, 20 microliters of the MTT solution (5 mg/ml in PBS; Sigma-Aldrich, USA) was added to each well, and the plates were incubated at the temperature of 37°C for an additional four hours in the dark.

After incubation, the medium was discarded, and 100 microliters of dimethyl sulfoxide (Sigma-Aldrich, USA) was added to each well in order to dissolve the purple formazan precipitate. The absorbance was measured using a microplate reader (Biotek, EON, USA) at the wavelength of 570 nanometers, and the viability rate was calculated using the following formula:

$$\text{Viability (\%)} = \left(\frac{A_{570 \text{ nm for Treated Samples}}}{A_{570 \text{ nm for Control Samples}}} \right) \times 100$$

Three independent experiments were performed on three different days. In each experiment, eight wells were used for each concentration. The half-maximal inhibitory concentration (IC₅₀) of the ZnO NPs in the cancer and normal cells was calculated using the Origin software (OriginPro 2016, USA).

NP cellular uptake assessment using ICP-MS

The cellular uptake of the ZnO NPs was

quantified using the inductively coupled plasma-mass spectrometry (ICP-MS). In total, 2×10^6 SKLC-6 and MRC-5 cells were seeded into the culture flasks and incubated at the temperature of 37°C for 24 hours. Afterwards, the cells were treated with 10 and 20 µg/ml of the ZnO NPs for another 24 hours; the concentrations were selected based on the NP cytotoxicity assessment. Non-treated cells were considered as controls.

After incubation, the cells were harvested via trypsinization and centrifuged at 3000 rpm for five minutes. Following that, the supernatant was removed, and the cells were washed twice with PBS and counted. The pellet was digested in concentrated nitric acid (HNO₃; Merck Chemicals, Germany) and diluted in five milliliters of Milli-Q water containing 2% HNO₃. The concentration of zinc was measured using the ICP-MS device (ELAN DRC-e, PerkinElmer Inc.). In addition, a solution containing single-element zinc was diluted in 2% trace metal-grade HNO₃ as the standard.

Irradiation setup

At this stage, the cells were irradiated using a 6-MV X-ray beam, which was generated by a medical linear accelerator (LINAC, Elekta, Stockholm, Sweden) with a dosimetric calibration based on the IAEA TRS 398 procedure [18]. The skin-source distance was set at 100 centimeters. The cell dishes were placed at the distance of 2-6 centimeters from the PTW water-equivalent slabs and tissue-equivalent bolus surrounding the dishes in order to consider the build-up and full backscatter conditions.

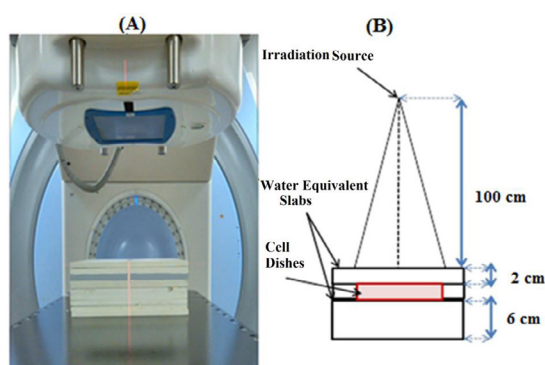


Fig 1. A) Photograph and B) Schematic View of Setup Used for Megavoltage Irradiation of Cells Using LINAC Device

The field size was set at 20 square centimeters, and the dose-rate at the position of the cells was 2 Gy/min. In addition, the absolute dose was measured using a calibrated ionization chamber

(PTW 30013, Germany). The daily uncertainty of the dosimetric measurements was $\pm < 1\%$. The photograph and a schematic view of the MV irradiation setup of the cells are depicted in Fig 1.

Radiosensitization assessment using the clonogenic survival assay

The radiosensitization effects of the ZnO NPs were assessed using the clonogenic survival assay, which is common method and a radiobiological ‘gold standard’ technique for the evaluation of radiosensitivity [19]. The SKLC-6 and MRC-5 cells were seeded into six-well plates at the density of 4×10^4 cells/well and incubated at the temperature of 37°C for 24 hours. Afterwards, the cells were treated with 10 and 20 µg/ml of ZnO NPs, and incubation continued for another 24 hours.

After incubation, the cells were exposed to a 6-MV X-ray beam in order to receive the graded doses of zero, two, four, six, and eight Gy. After four hours of incubation at the temperature of 37°C, the cells were washed twice with PBS, trypsinized, counted, and replated into six-well plates at proportional densities to the radiation dose. Following that, the cells were incubated in a humidified incubator for 12 days for colony formation. The colonies were stained with 0.4% crystal violet (Sigma- Aldrich, USA), and those with more than 50 cells were counted using inverted phase microscopy (CETI, Belgium). The plating efficiency (PE) and survival fraction (SF) of each group were calculated based on Equations one and two, as follows:

$$PE (\%) = \frac{\text{colonies number}}{\text{seeded cells number}} \times 100 \quad \text{Equation (1)}$$

$$SF = \frac{\text{colonies number}}{\text{seeded cells number} \times \%PE} \quad \text{Equation (2)}$$

Three experiments were performed independently in triplicate. Survival curves were generated by plotting the log SF versus the radiation dose and fitted to the linear-quadratic model (model: LQS; $SF = \exp^{-\alpha D - \beta D^2}$). In addition, the parameters of SF2 (survival fraction at 2 Gy), α (linear parameter of the survival curve, probability of lethal DNA damage), and β (quadratic parameter of the survival curve, probability of sub-lethal DNA damage) were extracted from the survival curves. Furthermore, the sensitizer enhancement ratio (SER) was calculated based on Equation three, as follows:

$$SER = \frac{MID_{IR}}{MID_{IR+ZnO NPs}} \quad \text{Equation (3)}$$

where MID_{IR} is the mean inactivation dose of the irradiated cells, and $MID_{IR+ZnO\ NPs}$ represents the mean inactivation dose of the irradiated cells treated with the ZnO NPs. MID was obtained using the area under the survival curve [20].

Evaluation of apoptosis using flow cytometry

The SKLC-6 and MRC-5 cells were seeded into six-well plates at the density of 4×10^4 cells/well and incubated for 24 hours. Afterwards, the cells were treated with 10 and 20 $\mu\text{g/ml}$ of ZnO NPs for 24 hours and exposed to the 2-Gy dose of the 6-MV X-ray beam. The cells were preserved in the incubator at the temperature of 37°C for another 24 hours.

Apoptosis induction in the cancer and normal cells was measured using the Annexin V-FITC apoptosis detection kit (Sigma- Aldrich, USA) in accordance with the instructions of the manufacturer.

After incubation, the supernatant medium containing floating cells was transferred to a falcon tube. Adherent cells were trypsinized and added to the preserved medium. Following that, the cells were collected via centrifugation, counted, and washed twice with PBS. In total, 5×10^5 cells were resuspended in 200 microliters of binding buffer (1 \times), and five microliters of Annexin V- FITC was added to each sample and incubated for 15 minutes at room temperature in the dark.

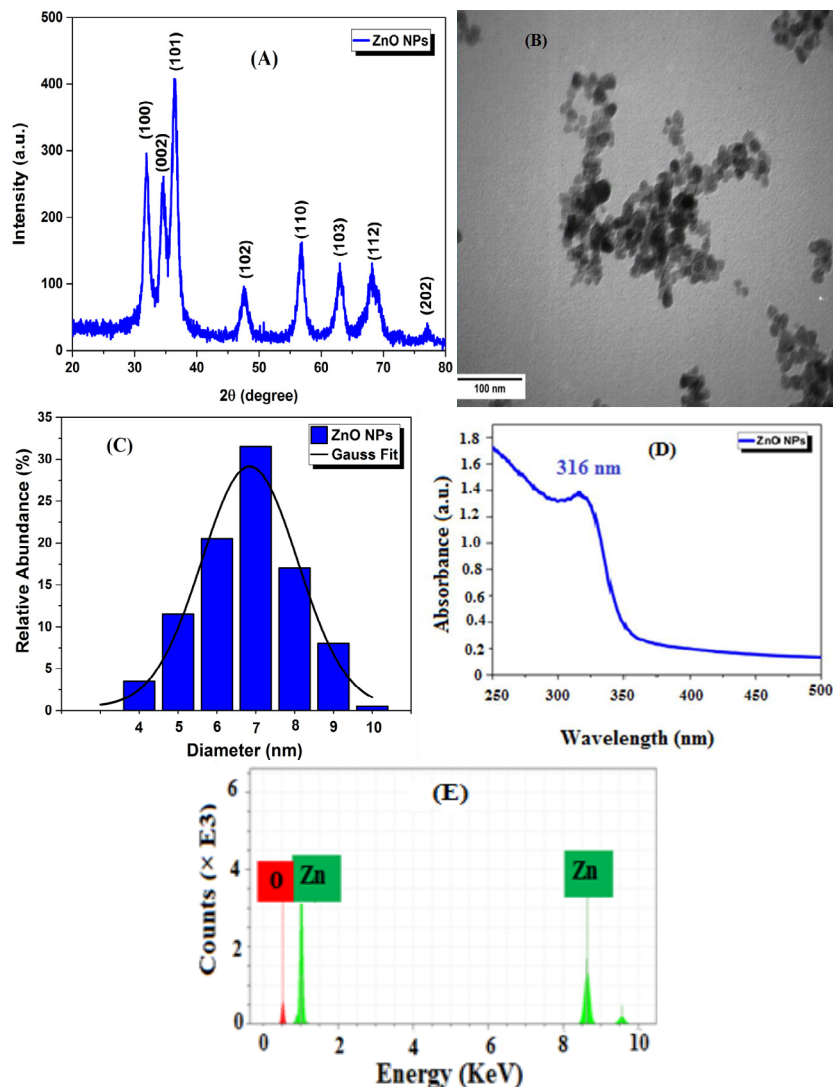


Fig 2. Characterization of Prepared ZnO NPs; A) XRD Pattern, B) TEM Image, C) Size Distribution, D) UV-Vis Spectrum, E) EDAX Spectrum

At the next stage, 10 microliters of PI (20 µg/ml) was gently added, and incubation continued for five minutes in the same conditions. Fluorescence measurement was performed using a FACSCalibur flow cytometer (Becton-Dickinson, Germany), and 10,000 calls per each sample were evaluated. The obtained data were analyzed using the BD Cell Quest Pro software.

Genotoxicity evaluation using the cytokinesis-block micronucleus assay (CBMN)

The SKLC-6 and MRC-5 cells were seeded into culture flasks at the density of 1×10^6 cells. After treatment with 10 and 20 µg/ml of ZnO NPs for 24 hours and exposure to the 2-Gy dose of the 6-MV X-ray, the cells were washed twice with PBS, and cytochalasin B (Sigma- Aldrich, USA) was added to each cell culture at the final concentration of 6 µg/ml. After 26-30 hours of incubation at the temperature of 37°C, the cells were resuspended in five milliliters of cold hypotonic solution (75 mM KCl) and fixed with a fixative solution (methanol: acetic acid: 3:1) for 10 minutes at room temperature. The fixation step was repeated twice. The final fixed cells were dropped onto pre-cooled glass slides and dried at room temperature. Prior to the microscopic analysis, the slides were stained with 10% Giemsa (Sigma-Aldrich, USA), and the cells counted under light microscopy (Nikon, YS100, Japan). The micronuclei rate (MNI %) was determined in 1,000 binucleated (BN) cells in each treatment in accordance with Fenech's criteria [21].

Statistical analysis

Data analysis was performed in SPSS version 16.0 (SPSS Inc. USA), and the results of the three independent experiments were expressed as mean and standard error of mean (SEM). One-way analysis of variance (ANOVA) and Tukey's multiple comparison test. The P-values of less than 0.001 (***), 0.01 (**), and 0.05 (*) were considered statistically significant. Moreover, the statistical significance in NP-treated and X-ray-treated groups WAS compared to the untreated control group, while in the groups receiving combination therapy (X-ray and NPs), the significance was compared to the X-ray-treated group.

RESULTS

Characterization of the ZnO NPs

The XRD pattern indicated seven distinct

peaks consistent with the lattice planes of (100), (002), (101), (102), (110), (103), and (200), as well as the pure single-phase hexagonal wurtzite structure of the ZnO NPs (JCPDS File No. 05-0664) (Fig 2-A). The TEM image revealed homogeneous spherical NPs with the mean size distribution of 7.34 ± 1.23 nanometers (Figs 2-B and 2-C). The UV-Vis spectrum indicated a characteristic absorption peak at 316 nanometers, which could be attributed to the excitonic absorption of the ZnO NPs (Fig 2-D) [22]. Furthermore, the EDAX spectrum confirmed that highly pure ZnO NPs were synthesized with no elemental impurities. The atomic rates of zinc and oxygen elements were estimated at 58.21% and 41.79%, respectively (Fig 2-E).

The hydrodynamic size of the prepared ZnO NPs in water was determined using DLS and estimated at 220 ± 43 nanometers. According to the findings, the dispersion of the ZnO NPs in PBS increased the hydrodynamic size of the ZnO NPs, while dispersion in DMEM decreased the hydrodynamic size of the ZnO NPs. Moreover, the hydrodynamic size of the ZnO NPs in the medium containing 10% FBS was lower than the medium containing 5% FBS (Table 1).

Table 1. Hydrodynamic Size and Zeta Potential of Dispersed ZnO NPs in Various Aqueous Media (Deionized Water, PBS, DMEM + 5% FBS, and DMEM + 10% FBS)

	Hydrodynamic Size (nm)	Zeta Potential (mV)
Deionized Water	220±43	27.0±1.5
PBS	355±26	-16.8±1.3
DMEM + 5% FBS	200±11	-27.2±1.6
DMEM + 10% FBS	142±32	-29.3±1.8

The zeta potential of the ZnO NPs in water was estimated at 27 ± 1.5 mV, indicating the cationic nature of the NPs. The dispersion of the ZnO NPs in PBS and DMEM led to the negative surface charge, which indicated the anionic nature of the NPs. In addition, the surface charge of the DMEM-dispersed ZnO NPs was more negative compared to the PBS-dispersed ZnO NPs. As such, the higher FBS content was observed to increase the negativity of the surface charge (Table 1).

The cytotoxicity profile and cellular uptake of ZnO NPs in the SKLC-6 and MRC-5 cells

To investigate the cytotoxicity profile of the ZnO NPs, the cancer and normal cells were treated with various concentrations of ZnO NPs for 24 hours, and the MTT assay was performed (Fig 3-A). In case of the cancer cells, 10 µg/ml, and in case of the normal cells, 20 µg/ml of the

ZnO NPs showed no significant toxicity compared to the untreated controls. After treatment with these concentrations, the ZnO NPs induced concentration-dependent toxicity in the cancer and normal cells. The calculated IC₅₀ values were 46.70±6.75 and 52.19±7.20 µg/ml in the cancer and normal cells, respectively, indicating the lower toxicity of the ZnO NPs in the normal cells compared to the cancer cells. In the subsequent experiments, two concentrations of ZnO NPs were selected, including 10 µg/ml as the sub-toxic concentration, and 20 µg/ml as the concentration that induced no higher cell toxicity than 20% according to Generalov et al [10].

In order to confirm the cellular uptake of the ZnO NPs, the cancer and normal cells were treated with 10 and 20 µg/ml of ZnO NPs for 24 hours, and the intracellular zinc content was quantified using the ICP-MS. As is depicted in Fig 3-B, the intracellular zinc content of the cancer cells increased approximately 1.5-fold (P<0.001) and two-fold (P<0.001) after treatment with 10 and 20 µg/ml of ZnO NPs, respectively compared to the control cells. In case of the normal cells, despite the increasing trend, the zinc content of the NP-treated cells showed no significant difference with the control cells (P>0.05).

Clonogenic survival assay

Fig 4 shows the clonogenic cell survival curves of the cancer and normal cells, as well as the images of colony formation in the cancer cells. The extracted parameters of the linear-quadratic (LQ) model fitted survival curves are presented in Table 2. According to the obtained results, ZnO NPs could effectively reduce proliferation, thereby increasing the sensitivity of the cancer cells to MV X-ray irradiation in a concentration-dependent manner, while exerting no significant effect on the radiosensitization of the normal cells (Figs 4-A and 4-B).

It is also notable that in the cases where NPs exhibited significant toxicity, the results were normalized to NP toxicity in order to eliminate the effects of NP toxicity [23].

As is observed in Fig 4-C, the colony-forming ability of the cancer cells reduced after exposure to the 2-Gy dose of X-ray.

The combination of 2-Gy X-ray and ZnO NPs induced further reduction in the number of the colonies, which was noticeable in the groups exposed to 2-Gy X-ray with 20 µg/ml of ZnO NPs.

According to the information in Table 2, the ZnO NPs significantly increased parameter α, while reducing parameter β and SF2 in the cancer cells.

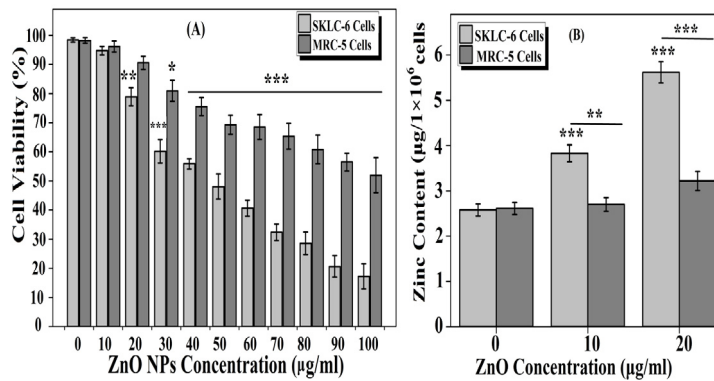


Fig 3. A) Cytotoxicity Profile, B) Cellular Uptake Analysis of ZnO NPs in SKLC-6 and MRC-5 Cells (Cells were untreated or treated with 10 and 20 µg/ml of ZnO NPs for 24 hours; NP cytotoxicity and intracellular zinc content measured using MTT assay and ICP-MS, respectively; Data expressed as mean±SEM of three independent experiments; *P<0.05, **P<0.01, ***P<0.001)

Table 2. Extracted and Calculated Parameters of LQ Model Fitted with Survival Curves of SKLC-6 and MRC-5 Cells (untreated or treated with ZnO NPs and exposed to 6-MV X-ray)

Treatment	SKLC-6 Cancer Cells			MRC-5 Normal Cells	
	α (Gy ⁻¹)±SEM	β (Gy ⁻²)±SEM	SF2±SEM	SER	SER
X-ray	0.072±0.006	0.030±0.001	0.76±0.007		
X-ray + ZnO NPs (10 µg/ml)	0.219±0.006	0.014±0.001	0.60±0.009	1.23	1.01
X-ray + ZnO NPs (20 µg/ml)	0.272±0.009	0.011±0.002	0.55±0.007	1.31	1.05

SF2: survival fraction at dose of 2 Gy; SER: sensitizer enhancement ratio

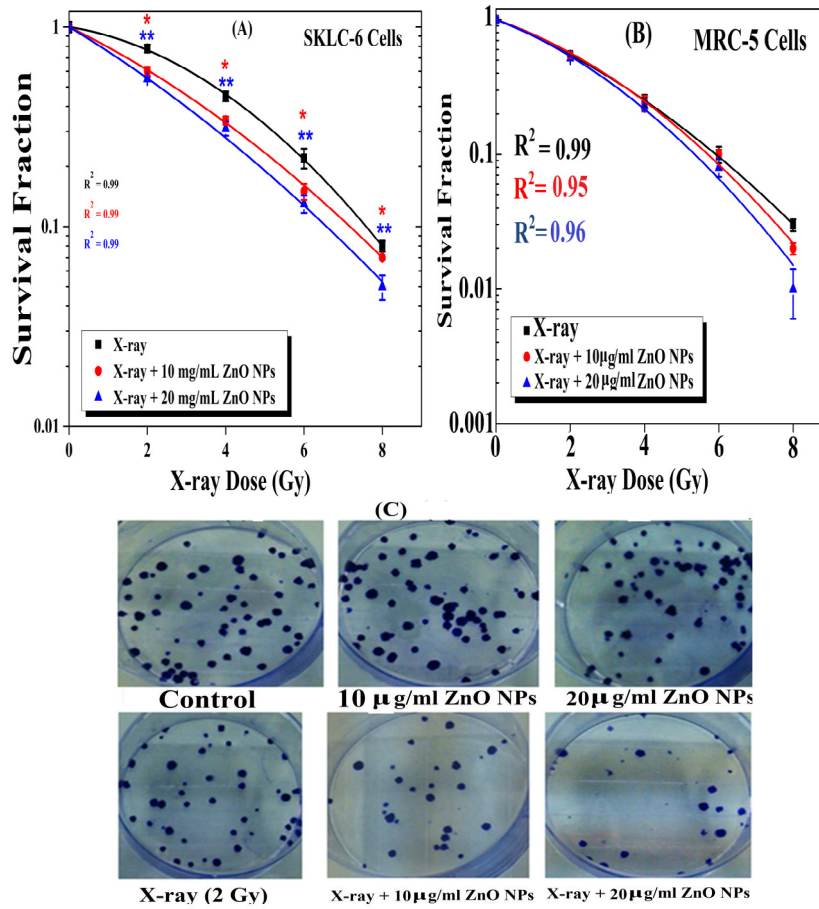


Fig 4. Clonogenic Cell Survival Curve of A) SKLC-6 Cells, B) MRC-5 Cells (untreated or treated with 10 and 20 µg/ml of ZnO NPs and exposed to various doses of 6-MV X-ray beam; Clonogenic cell survival curves fitted to the linear quadratic [LQ] model),C) Images of Colony Formation in SKLC-6 Cancer Cells with Various Treatments (Data expressed as mean±SEM of three independent experiments each performed in triplicate; *P<0.05, **P<0.01)

According to the SER results, the combination of X-ray with 10 and 20 µg/ml of ZnO NPs sensitized the cancer cells by approximately 23% and 31%, respectively, with no significant effect on the sensitivity of the normal cells (1 % and 5%, respectively). Therefore, it could be concluded that ZnO NPs could act as an effective selective radiosensitizer in high-energy X-ray irradiation.

Flow cytometry analysis of apoptosis induction in SKLC-6 and MRC-5 cells

In order to investigate apoptosis induction as a possible mechanism of radiosensitization by the ZnO NPs in 6-MV X-ray irradiation, fluorescence-activated cell sorting was performed on the SKLC-6 and MRC-5 cells.

The percentage of the apoptotic cells and scatter plots of apoptosis in the cancer and normal cells are shown in Figs 5A-C.

For apoptosis analysis, the apoptotic rate of the cells was considered as the sum of the cell populations in the lower right quadrant (LR), representing early-stage apoptotic cells and the upper right quadrant (UR), representing late-stage apoptotic cells.

As is depicted in Figs 5A-C, the presence of ZnO NPs in the high-energy X-ray field enhanced cell apoptosis induction in a concentration-dependent manner in the cancer and normal cells compared to the X-ray group (P<0.05).

However, apoptosis enhancement occurred at a higher rate in the cancer cells compared to the

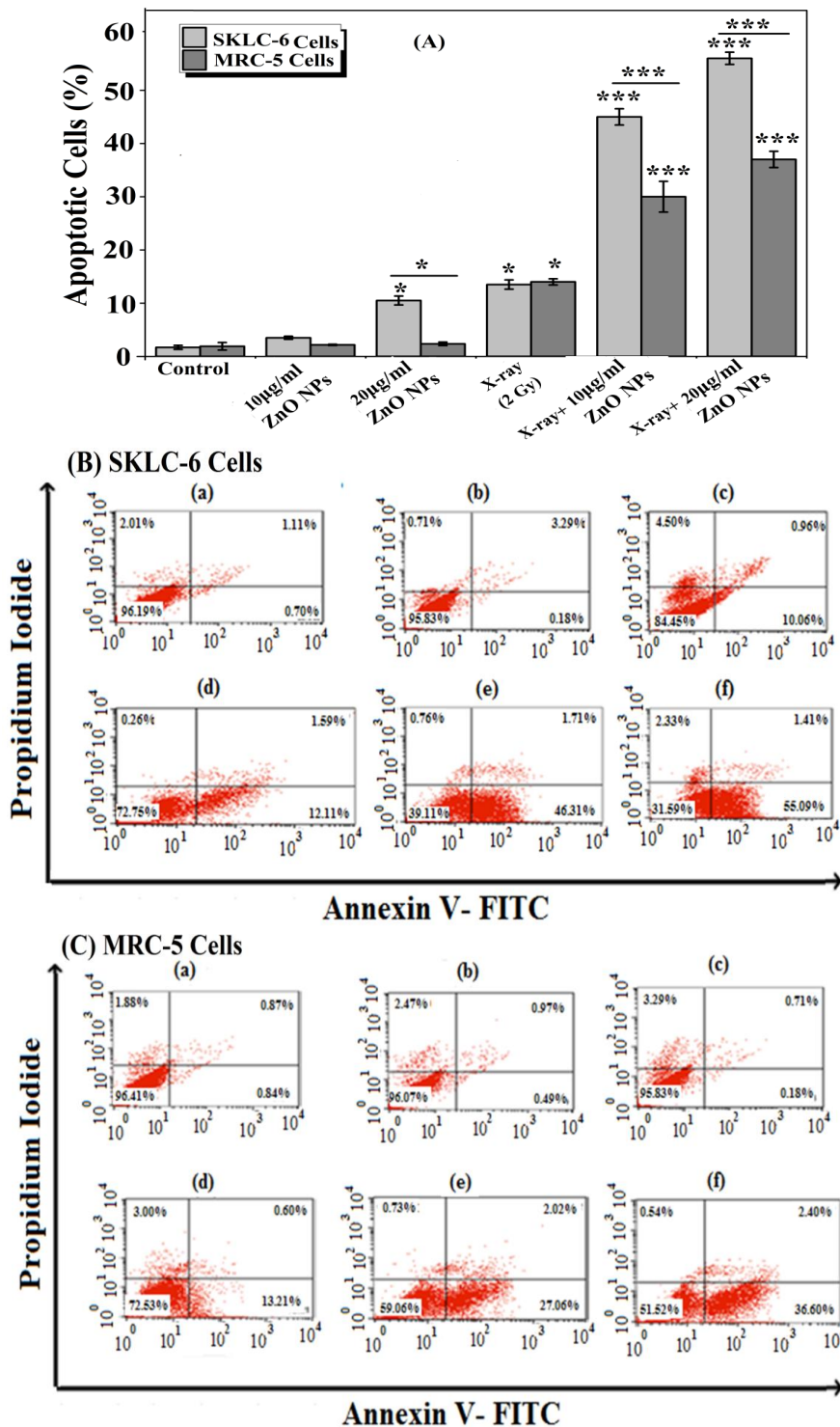


Fig 5. A) Flow Cytometry of Apoptosis Induction in Cancer and Normal Cells Based on Annexin V-FITC and PI Double Staining and Scatter Plots of Apoptosis in B) Cancer Cells and C) Normal Cells in a) Untreated Controls, b) Treatment with 10 µg/ml of ZnO NPs, c) Treatment with 20 µg/ml of ZnO NPs, d) X-ray (2 Gy), e) X-ray + 10 µg/ml of ZnO NPs, f) X-ray + 20 µg/ml of ZnO NPs (Data expressed as mean±SEM of three independent experiments; *P<0.05, **P<0.01, ***P<0.01)

normal cells ($P < 0.001$).

Genotoxicity assessment

The CBMN assay was performed on the SKLC-6 and MRC-5 cells in order to investigate the genotoxic effects of ZnO NPs as another possible radiosensitization mechanism in combination with high-energy X-ray, and MNi rate was determined (Fig 6).

The presence of the ZnO NPs in the X-ray field increased the MNi rate in the cancer and normal cells in a concentration-dependent manner, and the effect was exerted at a higher rate on the cancer cells compared to the normal cells. Therefore, it could be inferred that DNA damage is involved in ZnO NP radiosensitization.

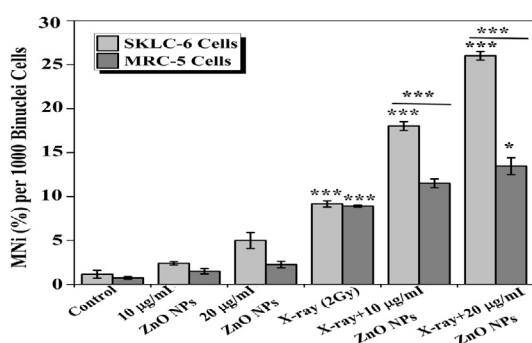


Fig 6. Micronuclei (MNi) Rate in SKLC-6 and MRC-5 Cells Measured by Cytokinesis-block Micronucleus (CBMN) Assay (Data expressed as mean \pm SEM of three independent experiments; * $P < 0.05$, *** $P < 0.01$)

DISCUSSION

Despite the major role of radiotherapy in numerous clinical settings, this approach has achieved limited success in the treatment of lung cancer due to its low specificity and non-selective nature [24]. Use of the radiosensitizers with a selective sensitizing ability could overcome the limitations of ionizing radiations, thereby improving the therapeutic efficacy of radiotherapy in patients with lung cancer. The current research aimed to investigate the possible selective radiosensitization effects of ZnO NPs on lung cancer cells under a 6-MV X-ray beam and further elucidate some of the cytotoxic and genotoxic mechanisms in this regard. To this end, ZnO NPs were synthesized using a chemical precipitation method as the most common, simple, and easily controlled synthesis route to obtain NPs with high purity and uniform nanocrystalline structures [25]. Characterization tests included XRD, TEM, UV-Vis, and EDAX, which confirmed the pure

crystalline structure of the ZnO NPs with narrow size distribution and the mean diameter of seven nanometers. These findings are consistent with the previous studies in this regard [16, 22].

The colloidal behavior or stability of NPs in aqueous media (especially physiological media) is an important issue in biomedical research. In the present study, the hydrodynamic size of the dispersed ZnO NPs in various aqueous media had higher values compared to TEM. This finding, which is in line with the previous studies [26-28], could be due to the differences in the measurement principles of the two applied methods. In DLS, the Brownian motion and the resulting distribution of a collection of the NPs that are dispersed in a suspension provide the mean hydrodynamic size, while in TEM, a dry layer of NPs on a grid is measured. During DLS measurements in the aqueous state, NPs tend to agglomerate, thereby showing the size of the clustered particles rather than the separate particles.

According to the results of the present study, PBS-dispersed ZnO NPs had larger hydrodynamic sizes compared to water-dispersed NPs. PBS is an isotonic buffered salt solution with a high concentration of phosphate ions [29]. The adsorption of phosphate ions onto the ZnO NP surface leads to the formation of zinc-phosphate complexes, which precipitate on the NP surface and result in the tendency of NPs to agglomerate [26, 30]. In contrast, the dispersion of ZnO NPs in the DMEM containing FBS was observed to decrease the hydrodynamic size and agglomeration tendency of the NPs. This finding is in congruence with the previous studies in this regard [26, 28].

In the current research, ZnO NPs exhibited potent protein adsorption properties [13]. The adsorption of the serum proteins with a negative surface charge onto the NP surface reduces the probability of particle-particle contact, as well as the possibility of NP agglomeration tendency. This effect is referred to as 'electrostatic stabilization' depending on the protein concentration, so that higher protein concentrations are associated with higher electrostatic stabilization. In the present study, the medium containing 10% FBS reduced the hydrodynamic size more effectively compared to the medium containing 5% FBS. Several reports have indicated that FBS at the routine concentration of 10% could promote the colloidal stability of NPs [26, 29].

In the current research, evaluation of the zeta potential showed that the ZnO NPs had a positive charge in water and a negative charge in physiological media (e.g., PBS and culture medium). This could be attributed to the adsorption of the protons with a positive charge from water, phosphate ions with a negative charge from PBS, and proteins with a negative charge from the culture media containing FBS. These findings are consistent with the other studies in this regard, which indicated that ZnO NPs are negatively charged in physiological media [26, 31]. Since the zeta potential of the dispersed ZnO NPs in DMEM with 10% FBS is close to the stability threshold of -30 mV, ZnO NPs could be considered electrostatically stable in DMEM with 10% FBS, which was used as a typical culture medium in the present study.

According to the present study, ZnO NPs induced dose-dependent cytotoxicity on the cancer and normal cells, while the effect was more evident in the cancer cells based on the MTT data; this is in line with the previous studies in this regard [32, 33]. Dissolution of ZnO NPs in intracellular components and the release of Zn²⁺ ions, which disrupt cellular zinc homeostasis and generate ROS, are considered to be among the major mechanism of ZnO NP cytotoxicity [13, 34]. In addition, the semiconductive properties of ZnO NPs and production of electrons and holes on the surface of NPs (even in the dark), which consequently lead to ROS generation, are another important mechanism associated with ZnO NP toxicity [32].

In the current research, ZnO NPs induced higher toxicity in the cancer cells compared to the normal cells. This finding is consistent with various studies in this regard [27, 35-37] and may have several reasons. For instance, the higher cellular uptake into cancer cells due to the attraction force between positively charged ZnO NPs and negatively charged plasma membrane of the cancer cells may be involved in the enhanced toxic effects on cancer cells [13]. However, our findings demonstrated that the ZnO NPs had a negative charge in the culture medium, and the effect may not be associated with the higher cytotoxicity of the cancer cells.

Another possible mechanism of the selective toxicity of ZnO NPs could be the cell proliferation rate [37]; cells with higher proliferation rates could uptake more NPs. In the present study, the

calculated doubling time of the SKLC-6 cancer cells and MRC-5 normal cells were estimated at 26.2 and 33.01 hours, respectively. Therefore, the higher cellular uptake in the cancer cells could be attributed to the higher proliferation rate of these cells compared to the normal cells. These findings were confirmed using the ICP-MS, implying that the intracellular zinc content of the cancer cells increased more significantly compared to the normal cells.

Low pH or the acidic extracellular environment of cancer cells play a pivotal role in the preferential toxicity of ZnO NPs toward cancer cells [38]. The extracellular microenvironment of cancer cells is acidic due to the accumulation of lactic acid, which is a product of glycolytic metabolism. The acidic environment leads to the rapid dissolution of ZnO NPs and release of the Zn²⁺ ions in the extracellular environment, which could uptake in cancer cells [38]. Consequently, the elevated levels of intracellular Zn²⁺ ions in cancer cells induce toxic effects.

In addition to the extracellular features of cancer cells, higher ROS and oxidative stress in cancer cells are considered to be another mechanism involved in the preferential toxicity in cancer cells [39]. Cancer cells have high levels of intracellular ROS due to high glycolytic metabolism and depleted antioxidant storage [39]. Therefore, the treatment of cancer cells with ROS generator agents (e.g., ZnO NPs) could induce more toxic effects compared to normal cells, which have normal levels of ROS and antioxidant storage [39].

According to the findings of the current research, 10 µg/ml of ZnO NPs in the cancer cells and 20 µg/ml in the normal cells were the sub-toxic concentrations of these NPs, which may have produced low levels of ROS that could be detoxified by cellular antioxidant machinery. It is well established that normal cells have a more efficient cellular antioxidant machinery to neutralize excessive ROS [39].

According to the data obtained from the clonogenic survival assay, the combination of ZnO NPs with 6-MV X-rays could preferentially reduce the proliferation rate and colony-forming ability of the cancer cells in a concentration-dependent manner (approximately 23% and 31% at the concentrations of 10 and 20 µg/ml, respectively). Interestingly, normal cells showed no significant sensitization. Therefore, it could be concluded that that use of ZnO NPs in the MV radiation field

could decrease the total radiation dose by up to 30%, thereby resulting in a significant reduction of side-effects in normal tissues.

The impact of the incident photon energy on the radiosensitization of various NPs (low- or high-Z nanomaterials) is a challenging issue, which has been addressed by numerous researchers [40-42]. In some cases, in addition to kV photons, MV photons have also been reported to induce significant radiosensitization [41, 43], while no radiosensitization effects have been observed upon MV irradiation in other cases [42]. The MV radiosensitization by ZnO NPs could be explained based on the high energy absorption in the NP structure, which in turn increases ROS generation. The spectrum of MV photons has a low-energy component [44], which could interact with ZnO NPs through photoelectric effects and generating low-energy photoelectrons and Auger electrons. It is notable that the probability of the photoelectric effects depends on the atomic number of the matter (Z^3).

The effective atomic number of ZnO is 26.9, while it is approximately 7.4 in the tissue. Therefore, the ratio of the probability of the photoelectric interaction with ZnO NPs compared to the tissue is approximately $48 (26.9/7.4)^3$. In other words, due to the interaction of X-rays with ZnO NPs, a large number of photoelectrons and Auger electrons are produced with the soft tissues. These low-energy, secondary electrons may excite ZnO NPs directly and lead to ROS generation or travel short distances outside the NPs, thereby depositing their energy into the surrounded molecules and generating free radicals [45]. On the other hand, the significant increase in the α parameter of the survival curves clearly indicated that the level of direct, lethal DNA damage increased in the presence of the ZnO NPs, which is similar to some high radiosensitization effects exerted by ZnO NPs [46, 47].

In a study in this regard, Generalov et al. reported that silica-coated ZnO NPs reduced the survival of LNCaP and Du145 human prostate adenocarcinoma cells approximately two-fold and 1.5-fold, respectively under X-ray irradiation (200 kVp) [10]. As expected, these values are higher compared to the values obtained in the present study due to the difference in the probability of the type of photon interactions.

Radiosensitization by NPs is a complex subject. In addition to radiation physics and localized

energy deposition, some biological mechanisms may be involved in this process [47]. In the current research, we assessed apoptosis induction and DNA damage as some of the possible biological mechanisms that may be involved in ZnO NP radiosensitization in combination with MV X-rays. According to the findings, ZnO NPs led to the 3-4-fold increase in the apoptosis rate of the cancer cells, while inducing lower apoptosis in the normal cells. Considering that apoptosis evasion is a hallmark of cancer development, induction of apoptosis results in therapeutic gain in cancer treatment. On the other hand, apoptosis induction enhances the tumor tissue responses to daily fractionated radiotherapy as the most common clinical radiotherapy regimen [48]. Some researchers have investigated ZnO NP-mediated apoptosis induction and the associated mechanisms *in-vitro* and *in-vivo* [49]. In general, it could be stated that ROS generation and severe damage to critical cell molecules are the key influential factors in the apoptosis induction by ZnO NPs, which activates various apoptotic signaling pathways, such as the *p53*, *survivin*, *bax/bcl-2*, and caspase pathways [50].

In addition to cytotoxic effects, the findings of the current research indicated that ZnO NPs induced genotoxic effects. Furthermore, DNA damage (micronuclei form) increased in combination treatments, and the effect was more significant in the cancer cells. Micronuclei originate from DNA strand breaks, forming dicentric chromosomes and acentric chromosome fragments [21]. The DNA damage potential of ZnO NPs and the associated molecular mechanisms have been investigated by many researchers; such example is a review study by Scherzad [51]. Using antioxidant agents to reduce the genotoxic effects of ZnO NPs has demonstrated that ROS generation and oxidative stress are the major triggers for the genotoxic effects of ZnO NPs [33].

In general, the results of the present study showed that ZnO NPs could act as a potent preferential radiosensitizer in the radiation therapy of lung cancer cells under high-energy X-ray irradiation. Some of the key advantages of ZnO NPs as proper radiosensitizers in combination with radiation therapy in the treatment of deep-seated lung tumors include selective function and relatively good discrimination between cancer and normal cells, potent radiosensitization effects, applicability in the actual clinical radiotherapy

of patients, low toxicity, biocompatibility, ease of synthesis, accessibility, and affordability. Moreover, ZnO NPs have been documented as effective agents in imaging contrast [12]. Therefore, they could be applied as theranostic agents to simultaneously induce dual effects in radiation fields.

To the best of our knowledge, this was the first study on the radiosensitization effects of ZnO NPs in combination with high-energy (6-MV) X-rays *in-vitro*, and there are no similar studies to compare the results.

Table 3 summarizes the results of some *in-vitro* studies performed on high-Z gold NPs as the most investigated radiosensitizers, as well as some low-Z NPs, such as titanium oxide and iron oxide (atomic numbers close to ZnO NPs) in combination with 6-MV X-rays, for the treatment of deep-seated tumors in clinical radiotherapy.

studies regarding NPsthere is no comparison with normal cells despite demonstrating potent radiosensitization effects. Considering that selective function is an important feature of an effective radiosensitizer, our findings indicated that ZnO NPs could selectively induce potent radiosensitization effects on the cancer cells, which confirmed their effectiveness as a radiosensitizer. It is also notable that the

ZnO NPs induced intrinsic, selective radiosensitization without specific targeting strategies. However, functionalization with targeting moieties could further improve the selectivity and toxicity of ZnO NPs against cancer cells [13].

CONCLUSION

The present study aimed to investigate the radiosensitization effects of ZnO NPs on lung cancer cells in combination with MV X-rays and determine some of the involved cytotoxic and genotoxic mechanisms in this regard. According to the results, ZnO NPs exerted significant preferential radiosensitization effects on the cancer cells (up to 30%). Furthermore, apoptosis induction and DNA damage were considered to be the underlying mechanisms that may be involved in the radiosensitizing effects of the ZnO NPs.

Therefore, it could be concluded that ZnO NPs in MV radiation fields could increase the clinical therapeutic efficacy of radiotherapy in the treatment of lung cancer.

ACKNOWLEDGMENTS

Hereby, we extend our gratitude to Tehran University of Medical Sciences, Tehran, Iran for the financial support of this research project (code: 95-04-30-33039).

REFERENCES

1. Bray F, Ferlay J, Soerjomataram I, Siegel RL, Torre LA, Jemal A. Global cancer statistics 2018: GLOBOCAN estimates of incidence and mortality worldwide for 36 cancers in 185 countries. *CA: Cancer J Clin.* 2018; 68(6): 394-424.
2. Hirsch FR, Scagliotti GV, Mulshine JL, Kwon R, Curran WJ, Jr., Wu YL, Paz-Ares L. Lung cancer: current therapies and new targeted treatments. *Lancet.* 2017; 389(10066): 299-311.
3. Chargari C, Riet F, Mazevet M, Morel E, Lepechoux C, Deutsch E. Complications of thoracic radiotherapy. *Presse Med.* 2013; 42(9 Pt 2): 342-351.
4. Salama JK, Vokes EE. New Radiotherapy and Chemoradiotherapy Approaches for Non-Small-Cell Lung Cancer. *J Clin Oncol.* 2013; 31(8): 1029-1038.
5. Wang H, Mu X, He H, Zhang XD. Cancer Radiosensitizers. *Trends Pharmacol Sci.* 2018; 39(1): 24-48.
6. Liu Y, Zhang P, Li F, Jin X, Li J, Chen W, Li Q. Metal-based NanoEnhancers for Future Radiotherapy: Radiosensitizing and Synergistic Effects on Tumor Cells. *Theranostics.* 2018; 8(7): 1824-1849.
7. Klein S, Sommer A, Distel LV, Neuhuber W, Krysch C. Superparamagnetic iron oxide nanoparticles as radiosensitizer via enhanced reactive oxygen species formation. *Biochem Biophys Res Commun.* 2012; 425(2): 393-397.
8. Morita K, Miyazaki S, Numako C, Ikeno S, Sasaki R, Nishimura Y, Ogino C, Kondo A. Characterization of titanium dioxide nanoparticles modified with polyacrylic acid and H₂O₂ for use as a novel radiosensitizer. *Free Radic Res.* 2016; 50(12): 1319-1328.
9. Juzenas P, Chen W, Sun YP, Coelho MA, Generalov R, Generalova N, Christensen IL. Quantum dots and nanoparticles for photodynamic and radiation therapies of cancer. *Adv Drug Deliv Rev.* 2008; 60(15): 1600-1614.
10. Generalov R, Kuan WB, Chen W, Kristensen S, Juzenas P. Radiosensitizing effect of zinc oxide and silica nanocomposites on cancer cells. *Colloid surface B.* 2015; 129: 79-86.
11. Zhang H, Patel N, Xiong J, Ding S. Targeting and noninvasive treatment of hepatocellular carcinoma in situ by ZnO nanorod-mediated concurrent chemoradiotherapy. *RSC Adv.* 2015; 5(104): 85720-85729.
12. Jiang J, Pi J, Cai J. The Advancing of Zinc Oxide Nanoparticles for Biomedical Applications. *Bioinorg Chem Appl.* 2018; 2018: 18.
13. Rasmussen JW, Martinez E, Louka P, Wingett DG. Zinc Oxide Nanoparticles for Selective Destruction of Tumor Cells and Potential for Drug Delivery Applications. *Expert Opin Drug Deliv.* 2010; 7(9): 1063-1077.
14. Ma H, Wallis LK, Diamond S, Li S, Canas-Carrell J, Parra A. Impact of solar UV radiation on toxicity of ZnO nanoparticles through photocatalytic reactive oxygen species (ROS) generation and photo-induced dissolution. *Environ Pollut.* 2014; 193: 165-172.

15. Lestari U, Mufti N, Lutfiyah DA, Fitriyah U, Annisa Y. UV Irradiation Enhanced In-Vitro Cytotoxic Effects of ZnO Nanoparticle on Human Breast Cancer. *J Phys Conf Ser.* 2018; 1093(1): 012046.
16. Ghaemi B, Mashinchian O, Mousavi T, Karimi R, Kharrazi S, Amani A. Harnessing the Cancer Radiation Therapy by Lanthanide-Doped Zinc Oxide Based Theranostic Nanoparticles. *ACS Appl Mater Interfaces.* 2016; 8(5): 3123-3134.
17. Baskar R, Lee KA, Yeo R, Yeoh K-W. Cancer and Radiation Therapy: Current Advances and Future Directions. *Int J Med Sci.* 2012; 9(3): 193-199.
18. AGENCY IAE. Absorbed Dose Determination in External Beam Radiotherapy. Vienna: IAEA; 2000.
19. Subiel A, Ashmore R, Schettino G. Standards and Methodologies for Characterizing Radiobiological Impact of High-Z Nanoparticles. *Theranostics.* 2016; 6(10): 1651-1671.
20. Jain S, Coulter JA, Hounsell AR, Butterworth KT, McMahon SJ, Hyland WB, Muir MF, Dickson GR, Prise KM, Currell FJ, O'Sullivan JM, Hirst DG. Cell-specific radiosensitization by gold nanoparticles at megavoltage radiation energies. *Int J Radiat Oncol Biol Phys.* 2011; 79(2): 531-539.
21. Fenech M. Cytokinesis-block micronucleus cytome assay. *Nat Protoc.* 2007; 2(5): 1084-1104.
22. Talam S, Karumuri SR, Gunnam N. Synthesis, Characterization, and Spectroscopic Properties of ZnO Nanoparticles. *ISRN.* 2012; 2012: 6.
23. Brun E, Sicard-Roselli C. Actual questions raised by nanoparticle radiosensitization. *Radiat. Phys Chem.* 2016; 128: 134-142.
24. Baker S, Dahele M, Lagerwaard FJ, Senan S. A critical review of recent developments in radiotherapy for non-small cell lung cancer. *Radiat Oncol.* 2016; 11(1): 115.
25. Kolodziejczak-Radzimska A, Jesionowski T. Zinc Oxide-From Synthesis to Application: A Review *Materials.* 2014; 7(4): 2833-2881.
26. Meißner T, Kathrin O, Potthoff A. Implications of the stability behavior of zinc oxide nanoparticles for toxicological studies. *Int Nano Lett.* 2014; 4: 116.
27. Akhtar MJ, Ahamed M, Kumar S, Majeed Khan MA, Ahmad J, Alrokayan SA. Zinc oxide nanoparticles selectively induce apoptosis in human cancer cells through reactive oxygen species. *Int J Nanomedicine.* 2012; 7: 845-857.
28. Bihari P, Vippola M, Schultes S, Praetner M, Khandoga AG, Reichel CA, Coester C, Tuomi T, Rehberg M, Krombach F. Optimized dispersion of nanoparticles for biological in vitro and in vivo studies. *Part Fibre Toxicol.* 2008; 5: 14.
29. Moore TL, Rodriguez-Lorenzo L, Hirsch V, Balog S, Urban D, Jud C, Rothen-Rutishauser B, Lattuada M, Petri-Fink A. Nanoparticle colloidal stability in cell culture media and impact on cellular interactions. *Chem Soc Rev.* 2015; 44(17): 6287-6305.
30. Ancona A, Dumontel B, Garino N, Demarco B, Chatzitheodoridou D, Fazzini W, Engelke H. Lipid-Coated Zinc Oxide Nanoparticles as Innovative ROS-Generators for Photodynamic Therapy in Cancer Cells. *Nanomaterials.* 2018; 8(3): 143.
31. Cho WS, Duffin R, Thielbeer F, Bradley M, Megson IL, Macnee W, Poland CA, Tran CL, Donaldson K. Zeta potential and solubility to toxic ions as mechanisms of lung inflammation caused by metal/metal oxide nanoparticles. *Toxicol Sci.* 2012; 126(2): 469-477.
32. Bisht G, Rayamajhi S. ZnO Nanoparticles: A Promising Anticancer Agent. *Nanobiomedicine (Rij).* 2016; 3: 9.
33. Pati R, Das I, Mehta RK, Sahu R, Sonawane A. Zinc-Oxide Nanoparticles Exhibit Genotoxic, Clastogenic, Cytotoxic and Actin Depolymerization Effects by Inducing Oxidative Stress Responses in Macrophages and Adult Mice. *Toxicol Sci.* 2016; 150(2): 454-472.
34. Shen C, James SA, de Jonge MD, Turney TW, Wright PF, Feltis BN. Relating cytotoxicity, zinc ions, and reactive oxygen in ZnO nanoparticle-exposed human immune cells. *Toxicol Sci.* 2013; 136(1): 120-130.
35. Reddy KM, Feris K, Bell J, Wingett DG, Hanley C, Punnoose A. Selective toxicity of zinc oxide nanoparticles to prokaryotic and eukaryotic systems. *Appl Phys Lett.* 2007; 90(213902): 2139021-2139023.
36. Hanley C, Layne J, Punnoose A, Reddy KM, Coombs I, Coombs A, Feris K, Wingett D. Preferential killing of cancer cells and activated human T cells using ZnO nanoparticles. *Nanotechnology.* 2008; 19(29): 295103.
37. Taccola L, Raffa V, Riggio C, Vittorio O, Iorio MC, Vanacore R, Pietrabbissa A, Cuschieri A. Zinc oxide nanoparticles as selective killers of proliferating cells. *Int J Nanomedicine.* 2011; 6: 1129-1140.
38. Sasidharan A, Chandran P, Menon D, Raman S, Nair S, Koyakutty M. Rapid dissolution of ZnO nanocrystals in acidic cancer microenvironment leading to preferential apoptosis. *Nanoscale.* 2011; 3(9): 3657.
39. Akhtar MJ, Alhadlaq HA, Kumar S, Alrokayan SA, Ahamed M. Selective cancer-killing ability of metal-based nanoparticles: implications for cancer therapy. *Arch Toxicol.* 2015; 89(11): 1895-1907.
40. Maggiorella L, Barouch G, Devaux C, Pottier A, Deutsch E, Bourhis J, Borghi E, Levy L. Nanoscale radiotherapy with hafnium oxide nanoparticles. *Future Oncol.* 2012; 8(9): 1167-1181.
41. Youkhana EQ, Feltis B, Blencowe A, Geso M. Titanium Dioxide Nanoparticles as Radiosensitisers: An In vitro and Phantom-Based Study. *Int J Med Sci.* 2017; 14(6): 602-614.
42. Khoshgard K, Hashemi B, Arbabi A, Rasaee MJ, Soleimani M. Radiosensitization effect of folate-conjugated gold nanoparticles on HeLa cancer cells under orthovoltage superficial radiotherapy techniques. *Phys Med Biol.* 2014; 59(9): 2249-2263.
43. Geng F, Song K, Xing JZ, Yuan C, Yan S, Yang Q, Chen J, Kong B. Thio-glucose bound gold nanoparticles enhance radiocytotoxic targeting of ovarian cancer. *Nanotechnology.* 2011; 22(28): 285101.
44. McMahon SJ, Hyland WB, Muir MF, Coulter A, Jain S, Butterworth KT, Schettino G, Dickson GR, Hounsell AR, O'Sullivan JM. Nanodosimetric effects of gold nanoparticles in megavoltage radiation therapy. *Radiother Oncol.* 2011; 100(3): 412-416.
45. Kleinauskas A, Rocha S, Sahu S, Sun YP, Juzenas P. Carbon-core silver-shell nanodots as sensitizers for phototherapy and radiotherapy. *Nanotechnology.* 2013; 24(32): 325103.
46. Detappe A, Kunjachan S, Rottmann J, Robar J, Tsiamas P, Kordeck H, Tillement O, Berbeco R. AGuIX nanoparticles as a promising platform for image-guided radiation therapy. *Cancer Nanotechnol.* 2015; 6(1): 4.
47. McMahon SJ, Hyland WB, Muir MF, Coulter JA, Jain S, Butterworth KT, Schettino G, Dickson GR, Hounsell AR, O'Sullivan JM, Prise KM, Hirst DG, Currell FJ. Biological consequences of nanoscale energy deposition near

- irradiated heavy atom nanoparticles. *Sci Rep.* 2011; 1:18.
48. Rupnow BA, Murtha AD, Alarcon RM, Giaccia AJ, Knox SJ. Direct evidence that apoptosis enhances tumor responses to fractionated radiotherapy. *Cancer Res.* 1998; 58(9): 1779-1784.
49. Saptarshi SR, Duschl A, Lopata AL. Biological reactivity of zinc oxide nanoparticles with mammalian test systems: an overview. *Nanomedicine (Lond).* 2015; 10(13): 2075-2092.
50. Vandebriel RJ, De Jong WH. A review of mammalian toxicity of ZnO nanoparticles. *Nanotechnol Sci Appl.* 2012; 5: 61-71.
51. Scherzad A, Meyer T, Kleinsasser N, Hackenberg S. Molecular Mechanisms of Zinc Oxide Nanoparticle-Induced Genotoxicity Short Running Title: Genotoxicity of ZnO NPs. *Materials.* 2017; 10(12).
52. Movahedi MM, Mehdizadeh A, Koosha F, Eslahi N, Mahabadi VP, Ghaznavi H, Shakeri-Zadeh A. Investigating the photo-thermo-radiosensitization effects of folate-conjugated gold nanorods on KB nasopharyngeal carcinoma cells. *Photodiagnosis Photodyn Ther.* 2018; 24: 324-331.
53. Hosseini V, Mirrahimi M, Shakeri-Zadeh A, Koosha F, Ghalandari B, Maleki S, Komeili A, Kamrava SK. Multimodal cancer cell therapy using Au@Fe₂O₃ core-shell nanoparticles in combination with photo-thermo-radiotherapy. *Photodiagnosis Photodyn Ther.* 2018; 24: 129-135.
54. Khoei S, Mahdavi SR, Fakhimikabir H, Shakeri-Zadeh A, Hashemian A. The role of iron oxide nanoparticles in the radiosensitization of human prostate carcinoma cell line DU145 at megavoltage radiation energies. *Int J Radiat Biol.* 2014; 90(5): 351-356.